Tensile Strength of Compacted Clays

Heibrock, G.[*], Zeh, R. M.[#], Witt, K. J.[#]

[*]*PHi Consult, Marburg, Germany*

[#]*Professorship of Foundation Engineering, Bauhaus-University Weimar, Germany*

(E-mail: rainer.zeh@bauing.uni-weimar.de)

SYNOPSIS - The paper presents experimental results linking matric suction and tensile strength of compacted clays. Test results from a cohesive soil are presented and discussed with respect to the soil structure and the interaction of soil and water. It is assumed that two main groups of pores can be clearly identified in compacted clays; the pores between aggregates (interaggregate pores) and pores between particles (intraaggregate pores). Based on a description of soil-water-interaction an expected behaviour, describing tensile strength as a function of matric suction, is derived and compared with the experimental results. The laboratory test results indicate that there is a strong correlation between the pore size distribution (assessed by interpretation of the soil water characteristic curve SWCC) and the tensile strength of compacted soils. Furthermore, the test results are compared by using micro-mechanical considerations of the interaction between the skeleton of unsaturated soils (interparticle contact force) and by using numerical calculations with an elastic relationship.

1. Introduction

Tensile strength of soils is usually not taken into account when dealing with soil related problems. Generally it is accepted that soils are not capable of resisting significant tensile forces over a longer time and there is almost no information on the influence of creep on the tensile strength of fine grained, i.e. clay, soils. Thus, the focus of the paper is not to investigate the meaning of tensile strength from an engineering point of view, but from a soil mechanics perspective. The results of some relatively simple investigations may contribute somewhat to the understanding and discussion on the soil water interaction and its meaning for the behaviour of fine grained soils used as compacted clay liners in landfills.

2. Soil Structure and Soil Water Interaction

Since the early days of clay colloid chemistry investigations (Endell, 1941) it is known that the engineering properties of fine grained soils are closely related to the soil water interaction. Investigations indicated that the amount of water that is absorbed by fine soils correlates to many properties of the soil (e.g. swelling behaviour, shear strength, compressibility etc.).

Fig. 2.1a (modified from Nagaraj et al., 1990) shows a schematic drawing of the fabric (arrangement of particles) of a fine grained soil. This kind of fabric is somewhat characteristic for a clay soil compacted dry of optimum (Proctor curve). Groups of clay particles are tied together and form aggregates of a 2 - 10 µm size. Pores between these aggregates (called interaggregate pores) usually show sizes clearly above 0,1 µm (10^{-7} m). The number and the size of interaggregate pores depend on the type of compaction and the water content at compaction (and indirectly on the suction). Jasmud & Lagaly (1993) and Nagaraj et al. (1986) showed that soil water is not bonded by clay particle surface forces (diffuse double layer forces, see Fig. 2.1c) at distances larger than about 6 x 10^{-9} m to particle surfaces. Therefore, water trapped in interaggregate pores will be considered as capillary water. It is assumed that interaction of soil and water can be described by the capillary theory in these pores.

Depending on the clay type, pore fluid chemistry, the soil preparation and the water content, the particles forming an aggregate show face to face, edge to edge or edge to face orientation. Pores inside the aggregates will be called intraaggregate pores and usually show sizes clearly below 0,1 µm. The number and size of these pores is not significantly influenced by compaction but from interparticle forces (Fig 2.1b, modified from Mitchell, 1993). Water trapped in intraaggregate pores is influenced by particle surface forces and capillary forces.

A clay soil compacted wet of optimum (Proctor curve) will show low volumes of interaggregate pores. Nevertheless, boundaries between aggregates, which form mechanically weak points exist. Fig. 2.1a gives an idea on the sizes of the mentioned elements. Note that the numbers have been taken from different but few sources, and therefore should be considered as orientation values.

The simple model will be used to derive an idea of the development of tensile strength of a compacted clay soil as a function of the water content. Taking into account the described bimodal pore structure it is assumed that the overall tensile strength is determined by forces which can be transmitted from aggregate to aggregate – since the tensile strength of the aggregates themselves will obviously be higher. Therefore, tensile strength of a compacted clay could be described by the tensile strength of an equivalent soil consisting of particles of the same size and shape as the aggregates (considering that these particles will decrease in size at lower water contents) and therefore, the capillary theory may be used to describe the process of tensile strength as a function of the water content.

Fig. 2.2 (taken from Schubert, 1982) shows the development of tensile strength of lime-stone. Starting from nearly saturated conditions the tensile strength t equals capillary pressure p_k times saturation S (capillary range). When pores begin to desaturate, tensile forces have to be transmitted by water bridges between

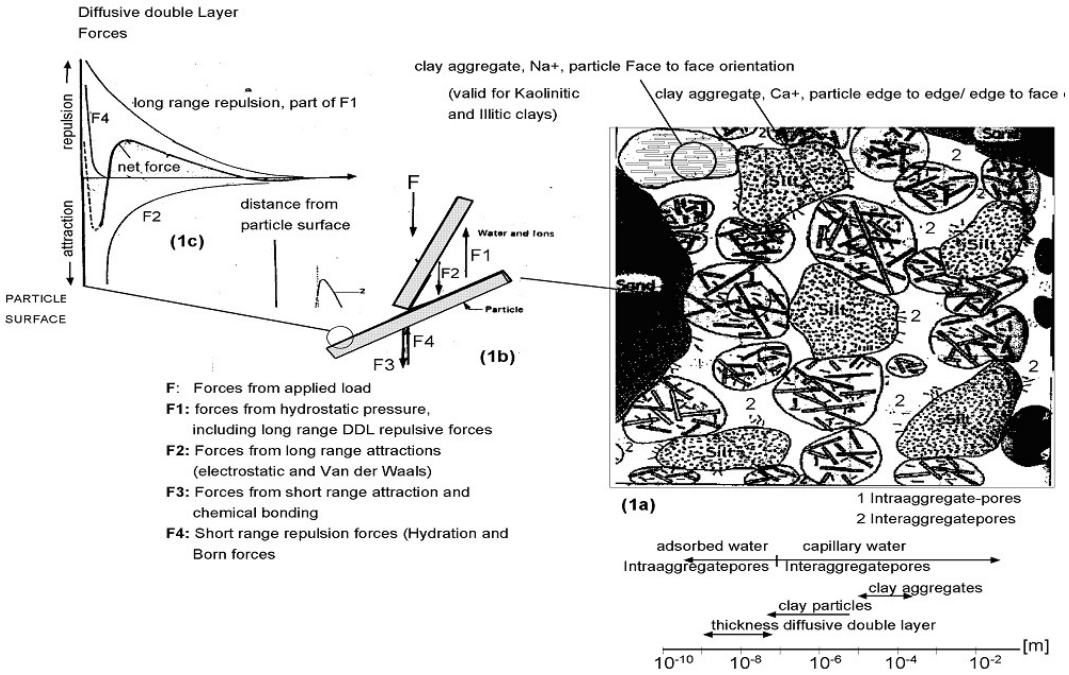

Fig. 2.1. Fine grained soil fabric (schematic) and water (modified from Nagaraj et al., 1990)

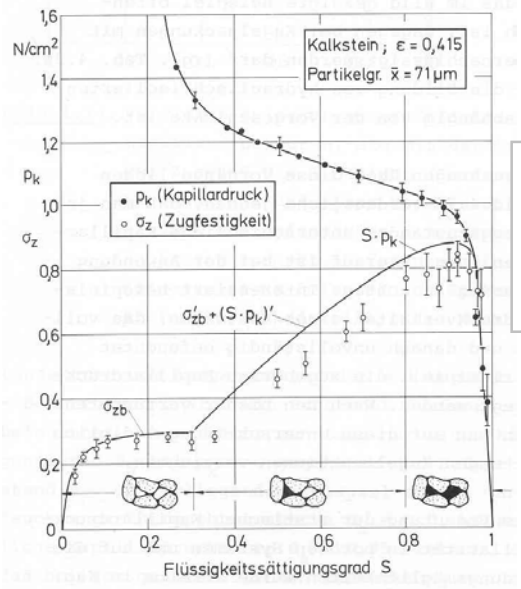

Translation

Flüssigkeitsgrad = degree of saturation
Kapillardruck = capillary pressure
Zugfestigkeit = tensile strength
Kalkstein = lime stone
Partikelgröße = particle size

Fig. 2.2. Tensile strength of a lime-stone (Schubert, 1982)

particles and still water filled pores. Schubert calls this stage the transition phase and he calculates the tensile strength as the sum of forces transmitted by water bridges σ_t and still saturated pores ($t = \sigma_t + (S \cdot p_k)$). When all pores have become desaturated the pendular state is reached and tensile strength is equal to σ_t.

Therefore, if we transfer this behaviour to compacted clay soils we should expect increasing tensile stresses with decreasing water contents reaching their maximum at a saturation of about 90 percent and decreasing tensile strength with further lowering of water contents.

3. Experimental Investigations

The following section describes sample preparation, the mode and results of direct tensile strength tests which were conducted by Brüggemann (1998). Furthermore, results are discussed with respect to the pore size distribution of the compacted soils assessed by interpretation of the soil water characteristic curve.

3.1 Sample Preparation and Test Procedure

Samples were Proctor compacted (3 layers compacted by 25 blows with 2,5 kg hammer) at optimum water content (e.g. 25,5 % gravimetric water content for the Kaolin samples). The sample of about 100 mm x 120 mm size was cut parallel to the layer surfaces preparing samples from the upper, middle and lower part. Be-

sides, the characteristic of the compaction differs over the height. Thus, differences in the soil structure and the tensile strength are expected for the samples (upper, middle and lower part). Each of the three samples is carefully trimmed using a wire-string creating three cylindrical samples of about 90 mm x 24 mm (height x diameter) size. At the end of this stage, the gravimetric water content of the samples is controlled by analysing soil residues from the trimming process. Water content losses up to 2% (related to the compaction stage) were observed. To investigate the influence of water content on tensile strength samples were air dried (at same conditions in a climatic chamber) or wetted (by spraying water on the sample surface, water content controlled by weighing the sample during the process). Subsequently, the samples were coated with wax to prevent further changes in the water content. In addition, the sample volume and hence the volumetric water content can be measured by dip-weighing. This is necessary to read the matric suction of the soil water characteristic curve measured separately from samples Proctor compacted at the same water content (middle part samples). The soil water characteristic curves were measured by Stoffregen (1997).

After wax coating the sample is stored in a climatic chamber for about 48 hours to ensure a homogeneous distribution of water in the sample. The final step is drilling bore holes of 8 mm diameter creating a hollow cylinder. A filter textile is placed in the centre of the sample, the right and left remaining part of the bore hole is filled with epoxy resin and two hooks are fastened with dowels placed in the bore holes. The reason for choosing the hollow-cylinder form is that maximum

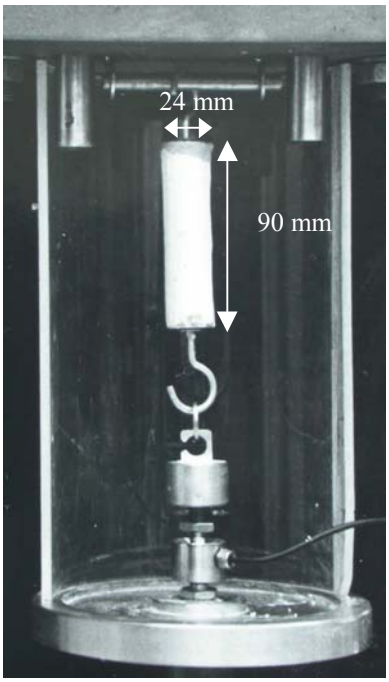

Fig 3.1. Sample and tensile strength test device

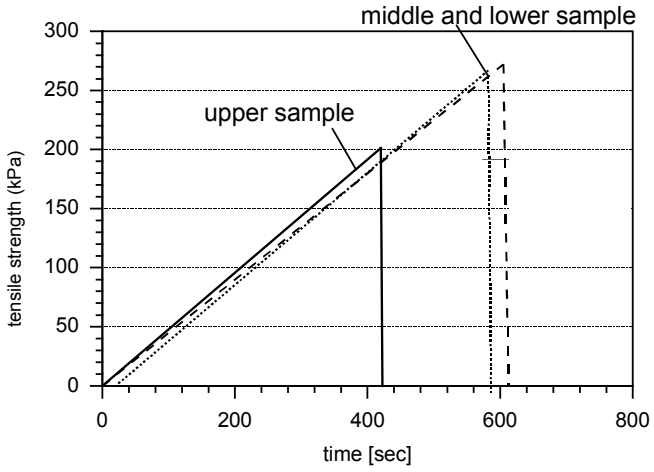

Fig. 3.2: Typical test result of the direct tensile strength test (test at 20% water content)

tensile stresses occur in the middle of the sample, and thus influences of 'spreading' forces to the sample are minimised (see results of elastic FE-calculations in section 4.3). Figure 3.1 shows a picture of the sample placed in the test device.

After carefully removing the wax coating the sample is placed in the test device (see Fig. 3.1) and is slowly torn apart (≅ 0,06 mm/min). Tests showed that lower velocities did not result in any changes in the measured tensile strength. During this process, tensile forces are measured. Fig 3.2 shows a typical test result. Tensile strength rises linearly with time as well as with strain until the sample rupture occurs. Axial tensile strength of the sample is defined as maximum tensile force measured during the test. Tensile strength is higher for samples taken from the lower part of the proctor sample indicating that compaction resulted in smaller interaggregate pores than in the middle and upper part of the proctor sample.

3.2 Test Results

The tests were conducted at a medium plastic clay (Kaolin clay - 61 % clay, 39 % silt; Proctor density 1,55 g/cm^3; Liquid limit 44,4 %, plastic limit 28,1%, shrinkage limit 25%, plasticity index 16,3 %, Proctor water content 25,5 %, activity 0,26). Figure 3.3 shows the parametrised soil water characteristic curve using a weighted sum of two Van-Genuchten functions (Durner, 1991):

$$\Theta = (\theta - \theta_r) / (\theta_s - \theta_r) = \sum w_i \, (1/(1 + \alpha \, (u_a - u_w))^{ni})^{mi} \quad (3.1)$$

where
Θ: water saturation [-], θ: volumetric water content [-],
θ_r: residual water content [-],
θ_s: volumetric water content at saturation [-]
w_i: weights [-]
u_a: pore air pressure [kPa], u_w: pore water pressure [kPa]
$u_a - u_w$: suction [kPa]
m_i, n_i : parameters [-], α : skaling [1/kPa].

$d\Theta/d\log(u_a - u_w)$ describes the change in saturation with a change in suction. Therefore, if a change in suction corresponds to a relatively large change in saturation this means that many pores desaturate at the applied suction. Thus, the maximum of $d\Theta/d\log(u_a - u_w)$ gives the pore size which is most frequent (filling

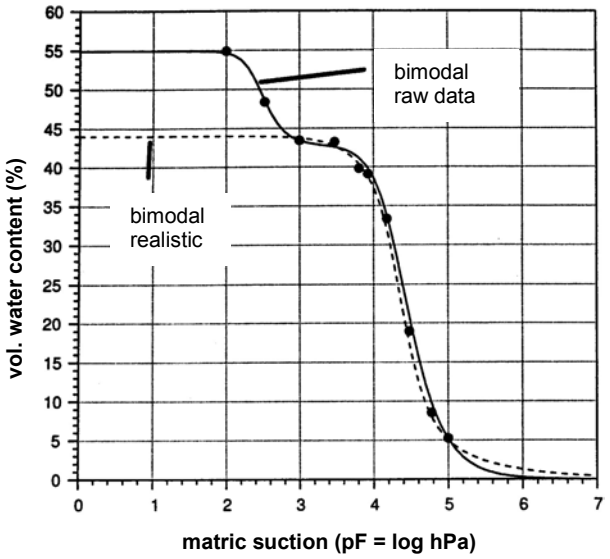

Fig. 3.3: Measured and parametrised soil water characteristic curve of Kaolin clay

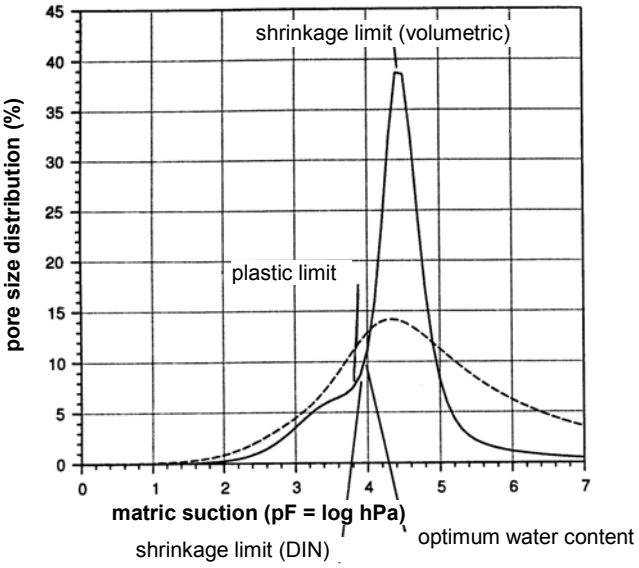

Fig. 3.4. Pore size distribution of Kaolin clay ($d\Theta/d\log(u_a - u_w)$)

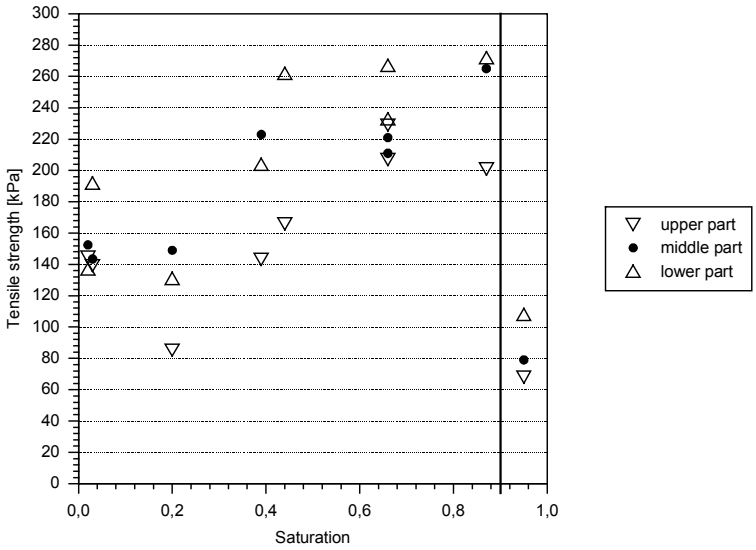

Fig. 3.5. Tensile strength as a function of suction

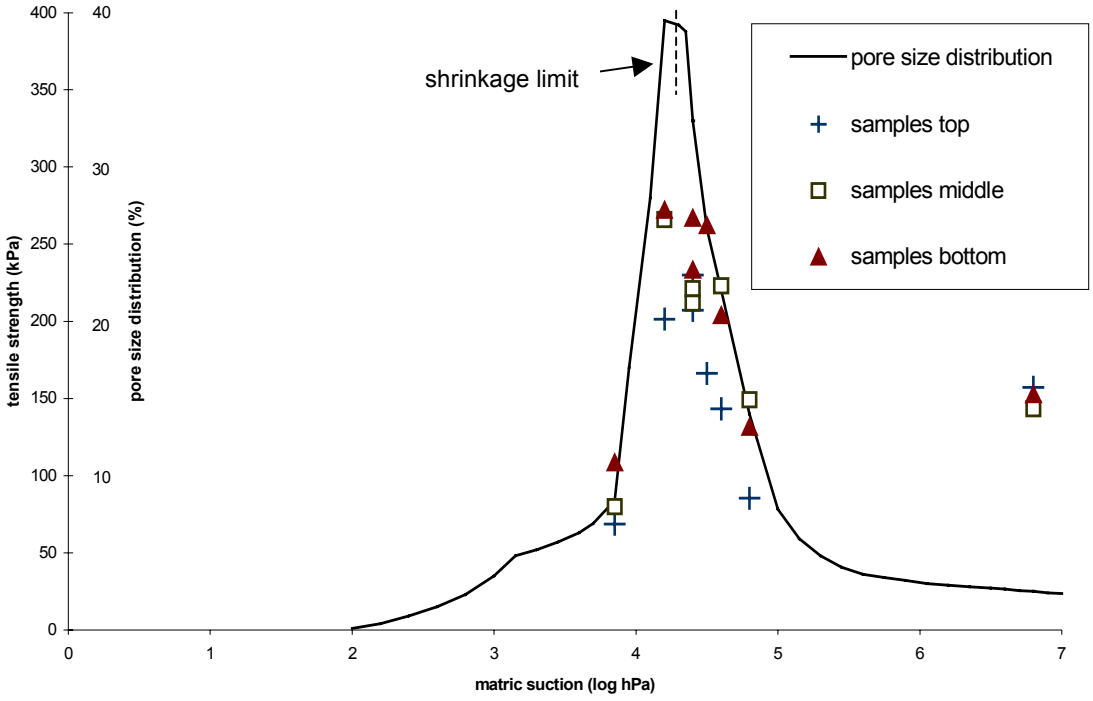

Fig 3.6. Pore size distribution and tensile strength of the compacted Kaolin

the largest volume) in the soil. Assuming that the soil pore system can be described as a bundle of capillary tubes of different sizes, $d\Theta/d\log(u_a - u_w)$ gives an idea of the distribution of capillary tube diameters and thus, the pore size distribution. Fig 3.4 shows the "pore size distribution" of Kaolin clay. Two regions can be identified. One region in the range of pF = 2 to about pF =4,5 (showing a maximum at pF = 4,2 – 4,3), which belongs to pore sizes larger than 0,1 μm (diameter calculated from capillary pressure) and therefore representing the water in the interaggregate pores. A second region ranging from about pF = 4,5 to about pF = 7 linked to pore sizes clearly lower than 0,1 μm and therefore representing water in the intraaggregate pores.

Figure 3.5 shows the results of tensile strength tests as a function of saturation (Brüggemann, 1998). The maximum value of tensile strength is reached at about 87 percent saturation corresponding to suctions of about pF = 4,3. Samples with lower water contents show decreasing values of the tensile strength, except the samples with lowest water content (gravimetric) of about 0,3 %. A slight reincrease of tensile strength can be identified. Generally, the samples taken from the upper part of the Proctor sample show lower tensile strengths than the samples from the middle and lower part.

Fig. 3.6 shows the measured tensile strength values as a function of suction combined with the "pore size distribution" of the Kaolin. In addition, the suction at shrinkage limit is marked. It can be seen that maximum tensile stress is reached at suctions just below the maximum of the pore size distribution which represents the most frequent interaggregate pores. This maximum corresponds to the shrinkage limit (determined by volumetric shrinkage tests). Thus, maximum tensile strength seems to occur when interaggagate pores are almost desaturated. The soil has left the normal shrinkage region, and forces between aggregates are transmitted more and more via water bridges. In terms of capillary theory (see section 2) this means that the soil develops from the transition to the pendular state. The next section deals with tensile forces calculated by means of the capillary theory assuming the pendular state.

4. Calculations and Comparison

According to the theory of porous solid systems (Schubert 1982, Heibrock, 1997, 1996), soil water in the pendular state occurs only in water bridges between the particles. Schubert (1982) and Molenkamp & Nazemi (2003) developed different approaches to calculate the forces between particles (smooth, rough) in the pendular state. Based on these approaches simple calculations of possible tensile strengths of homogeneous, undisturbed particle fabrics are presented, and show that the capillary theory gives the correct magnitude of tensile strength, when the pendular state is reached.

4.1 Interparticle Contact Forces

4.1.1 Calculations Based on Schubert (1982)

Schubert's calculations are theoretically based on the capillary theory of porous solid systems. In addition, different contact forms (e. g. identical spheres, spheres with different diameters, sphere to plate, etc.) are described in his book. Results of numerical calculations are combined in diagrams as shown in Fig. 4.1 b).

The following computations use i) the ratio of the water bridge volume and the sphere volume (V_l / V_s) and ii) the bridge angle β to read out the dimensionless contact force $F/\gamma \cdot x$ (compare with Fig. 4.1 a), where γ is the surface tension (for pure water and air, at a temperature of 293°K, the surface tension is $\gamma \cong 0{,}0727$ N/m) and x is the diameter of the sphere. Besides, the decisive tensile stress σ_t is derived from (Rumpf & Schubert, 1978)

$$\sigma_t = (1-e) \cdot F / e \cdot x^2 \qquad (4.1)$$

where e is the void ratio of the soil.

The Kaolin clay was used for all example calculations. The average void ratio of the samples is assumed as e = 0,6 (Brüggemann, 1998). The initial sphere diameter is usually 10 to 2 µm for a Kaolin, Snyder & Miller (1985) recommend an average diameter of 5 µm. After the shrinkage process, and consequently, for the

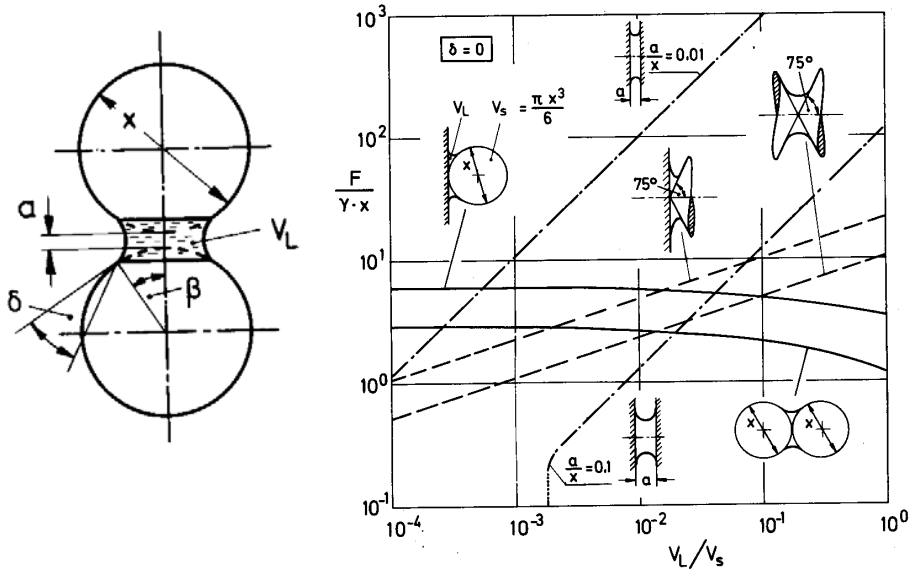

Figure 4.1. (a) Spheres with water bridge , (b) contact force versus contact forms and ratio of the water bridge volume and the sphere volume V_l / V_s (Schubert, 1982)

Table 4.1a. Tensile strength σ_t (kPa) versus contact form, ratio $V_l / V_s = 10^{-2}$ and diameter **x**

Form	x = 1,5 µm	x = 3,0 µm	x = 5,0 µm
	80,78	40,39	24,23
$x_1/x_2 = 2$	117,12	58,56	34,80
$x_1/x_2 = 10$	163,17	81,59	48,95
	190,64	95,32	57,19
	3231,11	1615,01	969,33

Table 4.1b. Tensile strength σ_t (kPa) versus contact form, ratio $V_l / V_s = 10^{-3}$ and diameter **x**

Form	x = 1,5 µm	x = 3,0 µm	x = 5,0 µm
	90,47	45,24	27,14
$x_1/x_2 = 2$	126,01	63,00	37,80
$x_1/x_2 = 10$	172,86	86,43	51,86
	203,59	101,80	61,07
	339,27	169,64	101,78

Table 4.1c. Tensile strength σ_t (kPa) versus contact form, ratio $V_l / V_s = 10^{-4}$ and diameter **x**

Form	x = 1,5 µm	x = 3,0 µm	x = 5,0 µm
	96,93	48,47	29,20
$x_1/x_2 = 2$	132,48	66,24	39,74
$x_1/x_2 = 10$	177,71	88,86	53,31
	210,02	105,01	63,01
	35,54	17,77	10,66

pendular state, a diameter of 1 to 3 µm is expected. Table 4.1a-c represents the results based on the described assumptions i) – the tensile strength versus the contact form, the ratio V_l / V_s and the diameter of the sphere.

Cohesive soils have naturally a mixture of the different contact forms (e. g. Mitchell, 1993). Therefore, a combination of the calculated contact form values (Table 4.1) could give similar tensile strengths as they were obtained by the laboratory tests.

The second calculation algorithm ii) uses the capillary pressure p_k (the suction) in the soil. By using the dimensionless capillary pressure $p_k \cdot x/\gamma$, the bridge angle β of the different sphere diameter is collected. According to that, the dimensionless force is collected likewise, then the tensile stress is calculated with equation 4.1.

The authors consider only sphere systems with the same diameter x, no other

Table 4.2. Tensile strength σ_t (kPa) versus diameter **x** (µm) and ratio of sphere distance **a/x**

	sphere distance a/x = 0	sphere distance a/x = 10^{-3}	sphere distance a/x = 0	sphere distance a/x = 10^{-3}
diameter x	bridge angle β (°)	bridge angle β (°)	σ_t (kPa)	σ_t (kPa)
2 µm	14,8	13,4	70,28	70,28
6 µm	8,6	7,6	24,23	23,02
20 µm	4,0	3,3	7,46	5,09
60 µm	1,8	1,5	2,52	0,87

Table 4.3. Tensile strength σ_t (kPa) versus grain size distribution

	proportional - grain size distribution Kaolin	sphere distance a/x = 0	sphere distance a/x = 10^{-3}
diameter x		σ_t (kPa)	σ_t (kPa)
2 µm	0,62	43,57	43,57
6 µm	0,24	5,82	5,53
20 µm	0,13	0,97	0,66
60 µm	0,01	0,03	0,01
	total sum	**50,39**	**49,77**

contact forms. As the suction value, 1995 kPa was chosen for the Kaolin (the shrinkage limit). The calculation results are represented in Table 4.2 by using two different ratios of sphere distance a/d (Fig. 4.1a). Table 4.3 shows the stresses according to the proportions of the grain size distribution of the Kaolin. It is evident that the size of the sphere distance a/d (at small values) does not play an important role for the tensile strength. The results are very similar.

4.1.2 Calculations Based on Molenkamp & Nazemi (2003)

Molenkamp & Nazemi (2003) consider the interactions between two rough spheres in detail (similar diameter, Fig. 4.2). These calculations ought to be compared to the computing for ii) above - the approach of Schubert. Fig. 4.2 shows the geometry of the problem. As a first value the dimensionless pressure differences

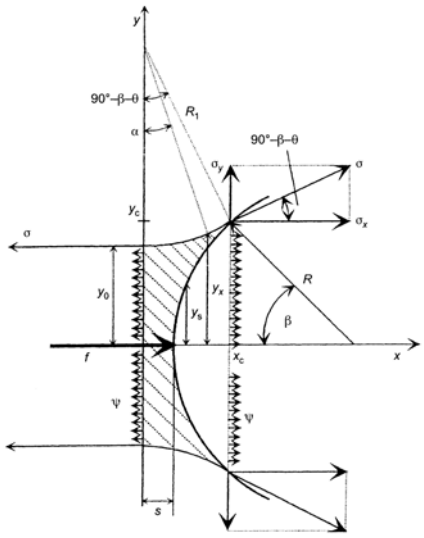

Fig. 4.2. Illustration of geometry of right-hand side of liquid bridge and actions on it (Molenkamp & Nazemi, 2003)

Table 4.4. Tensile strength σ_t (kPa) versus grain size distribution, a/x = 0 (a =2s, Fig. 4.2)

diameter x	contact force F (-)	proportional -grain size distribution - Kaolin	tensile strength σ_t (kPa)
2 µm	$1{,}6897\ 10^{-6}$	0,62	174,60
6 µm	$5{,}1064\ 10^{-6}$	0,24	22,70
20 µm	$1{,}2243\ 10^{-5}$	0,13	2,65
60 µm	$2{,}2224\ 10^{-5}$	0,01	0,04
		total sum	**199,99**

Table 4.5. Tensile strength σ_t (kPa) versus grain size distribution, a/x = 10^{-3} (a =2s, Fig. 4.2)

diameter x	contact force F (-)	proportional -grain size distribution - Kaolin	tensile strength σ_t (kPa)
2 µm	$1{,}2557\ 10^{-6}$	0,62	129,76
6 µm	$3{,}9942\ 10^{-6}$	0,24	17,75
20 µm	$8{,}3369\ 10^{-6}$	0,13	1,81
60 µm	$1{,}5479\ 10^{-5}$	0,01	0,03
		total sum	**149,35**

have to be obtained -

$$\psi = (u_a - u_w)\cdot x / \gamma \qquad (4.2)$$

whit $(u_a - u_w)\cdot$as suction, x as the diameter of the spheres and γ as the surface tension (in our example, the suction is 1995 kPa and the surface tension $\gamma \cong 0{,}0727$ N/m assuming a temperature of 293°K).

The force between the spheres is

$$F = f / x\cdot\gamma = \psi\pi Y_c^2 + 2\pi Y_c \sin(\beta+\theta) \qquad (4.3)$$

whith $Y_c = \sin\beta$, β as the bridge angle (Table 4.2). θ - the liquid-solid contact angle - is taken as 0. As above, the tensile strength is $\sigma_t = (1\text{-}e)\cdot F / e\cdot x^2$ and it is in accordance to the proportions of the grain size distribution of the Kaolin. The results of the calculations are represented in Table 4.4 and 4.5. Compared with the calculation results based on the approaches (ii) of Schubert (Table 4.3), higher tensile strengths are obtained.

4.2 Numerical Analyses

Simple numerical calculations with the FE-code COMPASS (Thomas et al., 2002), using the standard elastic relationship (Hook), showed the expected stress concentration in the middle of the hollow-cylinder-sample (Fig. 4.3) and parallel the contraction in the middle of the sample (see Fig 4.4). Typical soil parameter for the Kaolin clay were taken from Brüggemann (1998) and Alonso et al. (1990) - e. g. : n = 0,4, G = 3300 kPa, ν = 0,4.

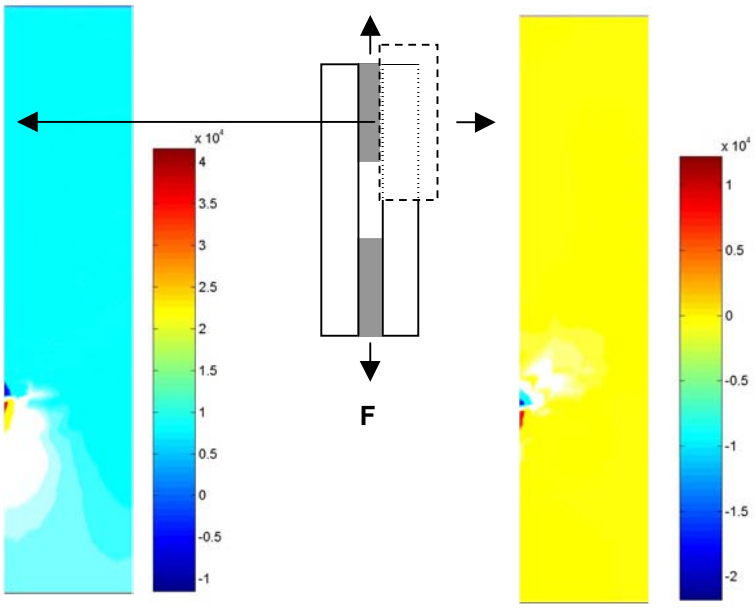

Fig. 4.3. a) Stress (Pa) in **y**-direction, sample scheme, b) in **x**-direction, after 122 s

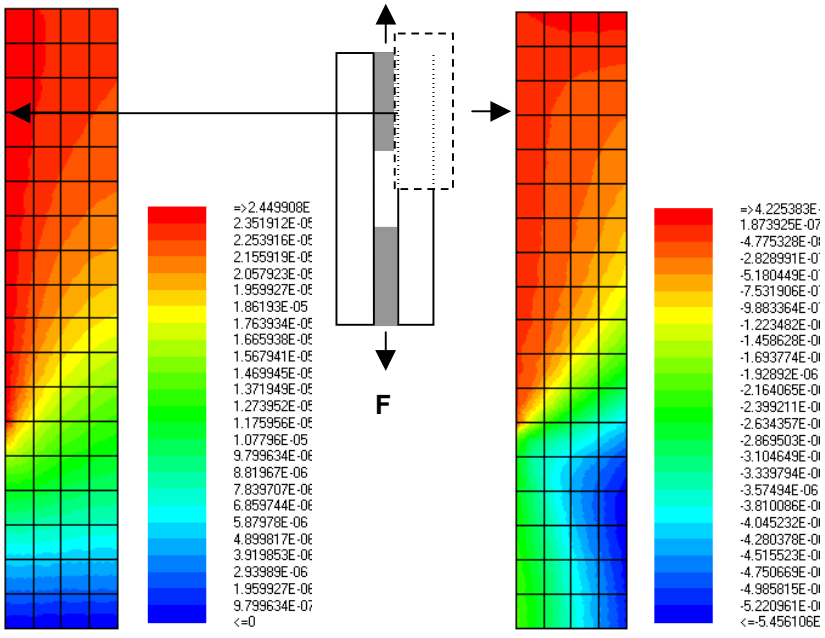

Fig. 4.4. a) Displacement (m) in **y**-direction, sample scheme, b) in **x**-direction, after 122 s

4.3 Comparison

The comparison of the test results in the laboratory and the analytic calculations based on the approaches of Schubert (1982) and Molenkamp & Nazemi (2003) shows that the correct magnitude of tensile strength could be obtained by using equations derived from the capillary theory. Obviously, the calculation of tensile strength as a product of 'total' saturation and suction overestimates tensile strength by an order of magnitude. In order to transfer the equations of Schubert / Molenkamp & Nazemi onto fine grained soils, the overall saturation S has to be replaced by S_I representing the degree of saturation of the interaggregate pores. Assuming that 7 % of the interaggregate pores remain saturated at pF = 4,3, where the maximum tensile strength was observed, the tensile strength calculated from $t = \sigma_t + (S_I \cdot p_k)$ equals 189 kN/m^2 – 289 or 339 kN/m^2 depending on the assumptions with respect to aggregate size distribution and contact form (see Tables 4.3 – 4.5). This range matches with the measured maximum values (see Fig. 3.5) although calculated tensile strength is about 20 % higher compared to the measured strength. This could be explained from the rough estimation of the still saturated part of the interaggregate pores. Assuming that the pendular state is reached at S = 0,2 and thus tensile stresses could be calculated only from forces transmitted by water bridges, the resulting tensile strength calculated from the equation of Schubert / Molenkamp & Nazemi equals 50 kN/m^2 – 140 or 200 kN/m^2 (see Tables 4.3 – 4.5) which again matches the observed values between 80 kN/m^2 and 140 kN/m^2. The equation of Molenkamp & Nazemi seems to give a better approximation indicating that contact forces between aggregates should be described by assuming rough contact conditions.

5. Conclusion

By now, the tensile strength's characteristics of compacted clays as a function of water content have been rarely investigated. Although the results documented above are not sufficient to confine the hypothesis that tensile strength of compacted clays could be explained by capillary theory assuming that tensile strength is governed by forces that could be transmitted at the boundaries between clay aggregates, the results indicate that the basic approach is promising.

The shape of the measured tensile strengths can be explained through the capillary theory as well as the magnitude of the measured values. This does not apply to very low water contents below saturation of 0,2.

Further investigations will take different soils (high and low plastic clays) into account, and attempts will be made to identify water volumes with different water contents which are trapped in interaggregate pores.

Acknowledgements

The second author acknowledges the support by the German Academic Exchange Service DAAD to his stay as a research visitor at the Geoenvironmental Research Centre GRC,

Cardiff University, United Kingdom. Thanks are also to Prof. H. R. Thomas and Dr. P. J. Cleall for their support and supervision.

References

Alonso, E. E., Gens, E., Josa, A. 1990. A constitutive model for partially saturated soils. Géotechnique 40, No. 4, pp. 405-430

Brüggemann, R. 1998. Zugfestigkeit verdichteter Tone als Funktion des Wassergehalts. Diplomarbeit. Institut für Grundbau und Bodenmechanik, Ruhr-Universität Bochum. unveröffentlicht

Durner, W. 1991. Vorhersage der hydraulischen Leitfähigkeit strukturierter Böden. Diss., Bayreuther Bodenkundliche Berichte, Band 20

Endell, K. 1941. Stand der Erkenntnisse über die Quellfähigkeit von Tonen, ihre innere Ursache und Bestimmung, Bautechnik, Heft 19, Berlin

Heibrock, G. 1996. Zur Rissbildung durch Austrocknung in mineralischen Abdichtungsschichten an der Basis von Deponien. Schriftenreihe des Instituts für Grundbau an der Ruhr-Universität Bochum, Heft 26

Heibrock, G. 1997. Desiccation cracking of mineral sealing liners. in: Proceedings Sardinia 1997, 6. International Waste Management and Landfill Symposium, CISA, Cagliari

Jasmund, K., Lagaly, G. 1993. Tonminerale und Tone: Struktur, Eigenschaften Anwendungen in Industrie und Umgebung. Stenkopff, Darmstadt

Mitchell, J. K. 1993. Fundamentals of Soil Behaviour. J. Wiley & Sons, London

Molenkamp, F., Nazemi, A. H. 2003. Interactions between two rough spheres, water bridge and water vapour. Géotechnique 53, No. 2, pp. 255 – 264

Nagaraj, T. et al. 1990. Discussion on « Change in pore size distribution due to consolidation of clays » by Griffith and Joshi, Géotechnique, Vol. 40 No. 2

Nagaraj, T., Murthy, S. 1986. A Critical reappraisal of compression index equations. Géotechnique 36, No. 1, pp. 27 – 32.

Rumpf, H., Schubert, H. 1978. Adhesion forces in agglomeration processes. in Onada & Hench: Ceramic processing before firing, J. Wiley a. Sons, Inc., London

Schubert, K. 1982. Kapillarität in porösen Feststoffsystemen. Springer Verlag, Heidelberg

Snyder, V. A., Miller, R. D. 1985. Tensile strength of unsaturated soils. Soil Sci. Soc. Am. J., Vol. 49: 58-65

Stoffregen, H. 1997. Bodenuntersuchungen an Kaolin. Fachgebiet der Bodenkunde und Regionale Bodenkunde, Institut für Ökologie, TU Berlin

Thomas, H. R., Cleall, P. J., Seetharam, S. C. 2002. Numerical modelling of the thermal-hydraulic-chemical-mechanical behaviour of unsaturated clay. Environmental Geomechanics. Monte Verità, pp. 125 - 136